Modeling, Simulation and Control for Optimized Operating Strategies of Combustion Engine-Based Power Trains

Andreas Rauh, Julia Kersten, Harald Aschemann
Chair of Mechatronics, University of Rostock, D-18059 Rostock, Germany
Email: {Andreas.Rauh, Julia.Kersten, Harald.Aschemann}@uni-rostock.de
Telephone: +49 381 498-9216, Fax: +49 381 498-9092

***Abstract*—In this paper, two different control-oriented modeling strategies are presented for the dynamics of a combustion engine-based power train. The first modeling approach corresponds to a so-called inverse model relating a given drive cycle to the mass flow of fuel and to the total fuel consumption. The alternative modeling approach represents a direct system description in which the fuel mass flow serves as the system input, while the resulting vehicle acceleration and velocity are the corresponding output variables. These models are employed for the optimization of operating strategies with respect to the fuel consumption and for the design of observer-based feedback controllers which are validated by numerical simulations. These controllers are designed in such a way as to allow for a real-time implementation of a velocity control approach. The presented system models as well as the corresponding optimization and control strategies are the basis for an experimental implementation on a test rig that is currently being built up at the Chair of Mechatronics at the University of Rostock.**

I. Introduction

Internal combustion engines are an integral component of most power train architectures for road and non-road vehicles. For that reason, a control-oriented modeling approach is presented in this paper. The modeling procedure can be subdivided into an inverse model that describes the interaction of the basic system components with the drive cycle as the system input and the fuel consumption that is required for its realization as the corresponding output. This type of system model has been taken into consideration in numerous related publications. Among these, especially the work of Guzzella has to be mentioned [1], [2]. His research led to the implementation of the MATLAB toolbox QSS [3] which has partly influenced the model architecture presented in this paper. The inverse modeling approach is characterized by the fact that dynamic component models can be evaluated algebraically. This holds as long as information concerning gear shifts is provided as a system input along with velocity and altitude profiles to characterize the vehicle's speed and operating conditions. From a system theoretic point of view, the purely algebraic computability of the inverse system model can be explained by the fact that the inverse model becomes differentially flat [4] under the above-mentioned assumptions.

This inverse system model is the basis for a model-based optimization of drive cycle parameters in the current paper. In contrast to [1]–[3], the gear shift information, however, is not provided as a system input. The gear shifts are rather determined during the evaluation of the inverse system model. This evaluation is based on a simplified dynamic gear box model which allows one to optimize drive cycle parameters and the angular velocities at which gear shifts have to be performed to achieve minimal fuel consumption. However, this extension leads to the drawback that the inverse model can no longer be evaluated in a purely algebraic manner. The optimization of drive cycle parameters is especially helpful for systems operating on the basis of a-priori known timetables. A typical example is the non-road application of combustion engines in railway vehicles [5], [6].

In addition to the inverse model, a direct system formulation is presented in this paper which contains exactly the same building blocks, however, with interchanged inputs and outputs. The direct model is employed for the derivation and implementation of observer-based control strategies that can be used in cruise control systems. In such applications, the fuel mass flow provided to the combustion engine is interpreted as the system input, while the vehicle's acceleration and velocity are the major output variables. Corresponding control strategies are derived in this paper, which are based on a reduced-order direct system model. The control procedures are validated by numerical simulations with a full-scale direct system model which reflects the system dynamics that are implemented as in the above-mentioned inverse system representation. Related research work, however, not using exactly inverted models for both the inverse and direct system representation can be found, e.g., in [7]–[9], where the advantage of using both directions of information flow simultaneously for optimization and control design are not exploited.

This paper is structured as follows. Section II gives an overview of both the inverse and direct system models. In addition, a conceptional design for a small-scale test rig is described which is currently being built up at the Chair of Mechatronics at the University of Rostock to validate operating strategies for combustion engine-driven and hybridized power trains. Optimization approaches and numerical results are presented in Section III with a focus on the minimization of fuel consumption. In Section IV, observer-based cruise control strategies are derived. The paper is concluded in Section V by an outlook on future work.

978-1-4673-2124-2/12/$31.00 ©2012 IEEE

II. Control-Oriented Modeling of Combustion Engine-Based Power Trains

In this section, both inverse and direct system models are derived for combustion engine-based power trains. As mentioned in the introduction, the first can be employed to quantify the effect of a predefined drive cycle on the fuel consumption, while the latter is used to compute the resulting drive cycle as the system output for a given fuel mass flow. In both cases, the mathematical descriptions consist of five components, representing the drive cycle, the vehicle, the gear box, the combustion engine with a quasi-static fuel consumption characteristic and a model for the fuel tank. The interaction between the different components is shown in Fig. 1. Here, the interface variables between the different system components are chosen in such a way that they reflect the power flow, for example, as a product of torque and angular velocity. The solid arrows denote the order of evaluation of the components for the inverse system model, while the dashed arrows correspond to the direct representation.

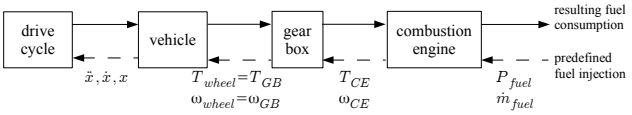

Fig. 1. Block diagram of the inverse and direct system representations.

Since the complete drive cycle is specified for the inverse model in terms of the acceleration and the speed of the vehicle, this model can be evaluated in a purely algebraic manner, as long as no dynamic models are introduced for the remaining components, that depend on internal state variables. Such internal variables become necessary, if the dynamic behavior is taken into account for selected components, such as for the automatic gear shift procedures described below. In contrast, the evaluation of the direct system model always corresponds to solving an initial value problem for a set of ordinary differential equations.

As an example, this property can be highlighted for the dynamics of the vehicle itself. In the case of a predefined drive cycle, where the speed $\dot{x}$ and the acceleration $\ddot{x}$ are given as system inputs, the resulting torque

$$T_{wheel} = \Big(F_{roll} + F_{air}(\dot{x}) + F_{grav} + F_{inert}(\ddot{x})\Big) \cdot r_{wheel} \quad (1)$$

at the wheels with the radius r_{wheel} is given by a purely algebraic expression, which depends on the rolling resistance F_{roll}, the velocity-dependent air resistance F_{air}, the downhill-slope force F_{grav}, and the inertia force F_{inert}. For the direct model, however, the torque T_{wheel} has to be transferred to the speed $\dot{x}$ by solving the differential equation

$$\ddot{x} = \frac{T_{wheel}}{m_{veh} \cdot r_{wheel}} - \frac{F_{roll}}{m_{veh}} - \frac{F_{air}(\dot{x})}{m_{veh}} - \frac{F_{grav}}{m_{veh}} \quad (2)$$

with the initial velocity $\dot{x}(t_0)$ and the vehicle mass m_{veh}. Details about all remaining component models are provided in the following Subsections II-A and II-B.

A. Inverse System Model

As mentioned above, the drive cycle represents the input for this type of model. In this paper, the discussion is restricted to analytic representations of a desired velocity profile consisting of three different phases, namely, acceleration, coasting (or driving with constant velocity), and deceleration. For this type of drive cycle, the time horizon $t \in [t_0 \,;\, t_f]$, $t_0 = 0$, and the total distance $s(t_f)$ are assumed to be predefined. Additionally, the acceleration and the speed are bounded by the intervals $\ddot{x} \in \left[\underline{\ddot{x}} \,;\, \overline{\ddot{x}}\right]$ and $\dot{x} \in \left[0 \,;\, \overline{\dot{x}}\right]$. The optimization routines described in the following section make use of a piecewise polynomial representation of the vehicle's velocity profile according to

$$\dot{x}_i = \sum_{j=0}^{3} \alpha_{ij} \cdot t^j \ , \quad (3)$$

where the phases $i \in \{A, B, C\}$ are defined in Fig. 2.

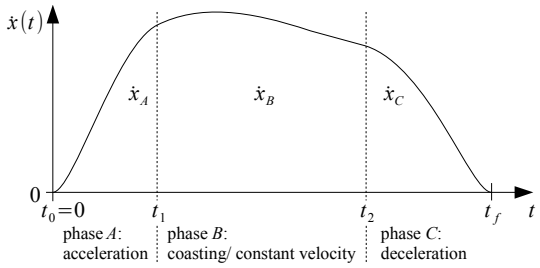

Fig. 2. Definition of a typical velocity profile.

Constraints on the coefficients α_{ij} are imposed by the specification of vanishing initial and final velocities

$$\dot{x}_A(0) = \dot{x}_C(t_f) = 0 \ . \quad (4)$$

Furthermore, continuity of the velocity and acceleration at the points of time t_1 and t_2 is represented by the constraints

$$\dot{x}_A(t_1) = \dot{x}_B(t_1) \quad \text{and} \quad \ddot{x}_A(t_1) = \ddot{x}_B(t_1) \quad (5)$$

as well as

$$\dot{x}_B(t_2) = \dot{x}_C(t_2) \quad \text{and} \quad \ddot{x}_B(t_2) = \ddot{x}_C(t_2) \ . \quad (6)$$

Constraints on the overall drive cycle length $s(t_f)$ are taken into account in a weak formulation by a suitable penalty term in the optimization routine described in the following section.

The speed and acceleration profiles $\dot{x}$ and $\ddot{x}$, respectively, serve as inputs for the subsequent component model, containing all external effects acting on the vehicle with the mass m_{veh}, the cross-section area A_{veh}, the drag coefficient c_w and the air density ρ. In addition, properties of the road are accounted for by the angle of inclination γ, the friction coefficient μ, and the gravitational constant g. The rolling resistance F_{roll}, the air resistance F_{air}, the downhill-slope force F_{grav}, and the inertia force F_{inert} in both the inverse model (1) and the direct model (2) are given by

$$F_{roll} = m_{veh} \cdot g \cdot \cos\left(\gamma(x)\right) \cdot \mu \ , \quad (7)$$

$$F_{air} = \frac{1}{2} \rho \cdot c_w \cdot A_{veh} \cdot \dot{x}^2 \ , \quad (8)$$

$$F_{grav} = m_{veh} \cdot g \cdot \sin\left(\gamma(x)\right) \quad , \quad \text{and} \tag{9}$$

$$F_{inert} = m_{veh} \cdot \ddot{x} \ . \tag{10}$$

Using the equations above, and the relation $\omega_{wheel} = \frac{\dot{x}}{r_{wheel}}$ for the angular velocity of the wheels, the gear box model can be employed to relate the variables $\omega_{wheel} = \omega_{GB}$ and $T_{wheel} = T_{GB}$ to the corresponding angular velocity and torque on the combustion engine's side with the corresponding gear ratio λ. Here, the relations $\omega_{CE} = \lambda \cdot \omega_{GB}$ and $T_{GB} = \lambda \cdot T_{CE}$ hold for a fixed gear ratio λ.

To automatically perform gear shifting during evaluation of the drive cycle, the following gear box model including an underlying control loop is taken into consideration. The control loop is designed in such a way to prevent violations of the maximum admissible angular velocity and the maximum admissible torque of the internal combustion engine. Violations of the operating range for the admissible velocity range are prevented by a suitable choice of the values λ for each gear number i_{GB}, while violations of the torque characteristic can only be avoided by a limitation of the variation rate $\dot{\lambda}$ of the transmission ratio during the shifting process. An example is shown in Fig. 3, where the torque $T_{inert}(\dot{\omega}_{CE}) = J_{CE} \cdot \dot{\omega}_{CE}$, resulting from acceleration and deceleration of the combustion engine during gear shifting has to be bounded such that

$$T_{idle} \leq T_{CE}(\omega_{CE}) \leq \overline{T}_{CE}(\omega_{CE}) \tag{11}$$

holds. For that purpose, the engine torque balance

$$T_{CE}(\omega_{CE}) = \frac{1}{\lambda} \cdot T_{GB}(\omega_{CE}) + T_{inert}(\dot{\omega}_{CE}) \tag{12}$$

is considered during gear shifting.

Here, the torque $T_{CE}(\omega_{CE})$ is the one that is actually being provided by the combustion engine, while $T_{inert}(\dot{\omega}_{CE})$ accounts for the engine's mass moment of inertia J_{CE}. The lower bound in (11) corresponds to the idling torque of the motor. For operating points below this line in Fig. 3, active braking of the vehicle is required (torque $T_{brake} < 0$)). If the upper bound $\overline{T}_{CE}(\omega_{CE})$ becomes critical, the variation rate $\dot{\lambda}(t)$ has to be limited according to the following procedure.

By considering the time derivative of the engine's angular velocity

$$\dot{\omega}_{CE}(t) = \dot{\lambda}(t) \cdot \omega_{GB}(t) + \lambda(t) \cdot \dot{\omega}_{GB}(t) \tag{13}$$

and substituting it into (12), the relation

$$\dot{\lambda}(t) \leq \frac{-\lambda \cdot \dot{\omega}_{wheel} + \frac{-\frac{1}{\lambda} \cdot T_{wheel} + \overline{T}_{CE}(\lambda \cdot \omega_{wheel})}{J_{CE}}}{\omega_{wheel}} =: \dot{\bar{\lambda}}(t) \tag{14}$$

can be derived. To satisfy this inequality, the gear ratio λ is determined during the shifting process by a PI-control law

$$\lambda_{PI}(t) = K_R \cdot \left(\Delta\lambda(t) + \frac{1}{T_N} \int_0^t \Delta\lambda(\tau)\, d\tau \right) \tag{15}$$

with $\Delta\lambda(t) = \lambda_f(i_{GB}) - \lambda(t) + \Delta\lambda^*$, $\lambda(0) = \lambda(i_{GB}(0))$, where $\lambda(i_{GB})$ is the steady-state gear ratio corresponding to i_{GB}. The desired gear ratio $\lambda(i_{GB})$ is filtered by a second-order lag element to guarantee smooth switching processes. The corresponding filtered output signal is denoted by $\lambda_f(i_{GB})$. With this information, the admissible gear ratio is obtained by

$$\lambda(t) = \lambda(0) + \int_0^t \dot{\lambda}_{GB}(\tau)\, d\tau \tag{16}$$

with

$$\dot{\lambda}_{GB}(t) = \begin{cases} \dot{\lambda}_{PI}(t) & \text{if } \dot{\lambda}_{PI}(t) \leq \dot{\bar{\lambda}}(t) \text{ holds} \\ \dot{\bar{\lambda}}(t) & \text{else} \ . \end{cases} \tag{17}$$

To prevent the effect of integrator windup, the term $\Delta\lambda^* = K_{aw} \cdot \left(\dot{\lambda}_{PI}(t) - \dot{\bar{\lambda}}(t) \right)$ is included in the control law (15).

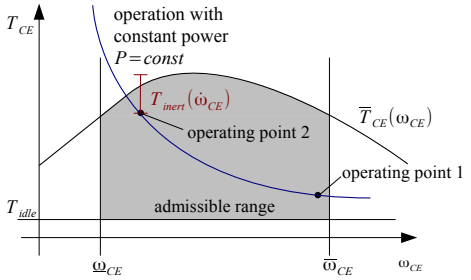

Fig. 3. Definition of the operating range for the combustion engine while gear shifting between two operating points with identical power demand.

Note that gear shifting is only performed at discrete points of time t_k with a fixed sampling rate $t_{k+1} - t_k$. Depending on the current gear number $i_{GB}(t_k) \in \{1, \ldots, 5\}$, the shifting strategy is given by

$$i_{GB}(t_{k+1}) = \begin{cases} i_{GB}(t_k) + 1 & \text{for } \omega_{CE} > \overline{\omega} \text{ and } i_{GB}(t_k) < 5 \\ i_{GB}(t_k) - 1 & \text{for } \omega_{CE} < \underline{\omega} \text{ and } i_{GB}(t_k) > 1 \\ i_{GB}(t_k) & \text{else} \ . \end{cases} \tag{18}$$

Finally, the dynamics of the combustion engine is described. It mainly consists of a quasi-static fuel consumption map which relates the engine's steady-state torque $\tilde{T}_{CE}$ and the angular velocity ω_{CE} to the fuel mass flow $\dot{m}_{fuel}(t)$. To make this model more realistic, a dead time element, representing the filling up of the cylinders, and a first-order lag element covering delays introduced by the finite volume of the suction pipe are assumed to describe the relation between the actual motor torque T_{CE} and its steady-state value $\tilde{T}_{CE}$ according to the transfer function

$$G_{CE}(s) = \frac{T_{CE}(s)}{\tilde{T}_{CE}(s)} = \frac{e^{-T_t s}}{(T_D s + 1)} \ . \tag{19}$$

To obtain a causal, invertible, minimum-phase approximation, the dead time element is approximated by a first-order lag element with a further extension by two lead elements for which $\tilde{T} > 0$, $\tilde{T} \ll T_t$, $\tilde{T} \ll T_D$ holds. This leads to the transfer function

$$G_{CE}(s) \approx \frac{(\tilde{T} s + 1)^2}{(T_D s + 1)(T_t s + 1)} \tag{20}$$

with

$$G_{CE}^{-1}(s) \approx \frac{(T_D s+1)(T_t s+1)}{(\tilde{T}s+1)^2} \tag{21}$$

which is used for the evaluation of the inverse system model. The overall fuel consumption (corresponding to the fuel tank model) can be determined easily by integration of the mass flow resulting from the consumption map depicted in Fig. 4(a) with respect to time.

B. Implementation of the Direct System Model

The direct system model consists of exactly the same system components that were introduced in the previous subsection. As already mentioned, algebraic component models such as the one representing the vehicle's dynamics turn into sets of ordinary differential equations during this model inversion. The vehicle model is now given by (2), where the resulting velocity profile $\dot{x}(t)$ and the distance $x(t)$ are computed as the solution to an initial value problem. The previously introduced gear box model — which has already been given in terms of a dynamic representation in the inverse model — remains unchanged.

Finally, the inverted combustion engine model makes use of the torque characteristic shown in Fig. 4(b). In analogy to the fuel consumption map in Fig. 4(a), it is possible to describe this quasi-static dependency by a polynomial approximation. Moreover, the transfer function $G_{CE}(s)$ is now used instead of $G_{CE}^{-1}(s)$ to determine the input torque of the gear box which is further transferred to the torque acting onto the vehicle. The combustion engine characteristics in Figs. 4(a) and 4(b) are taken from [3]. They are scaled according to the power and velocity range of the test rig that is described subsequently.

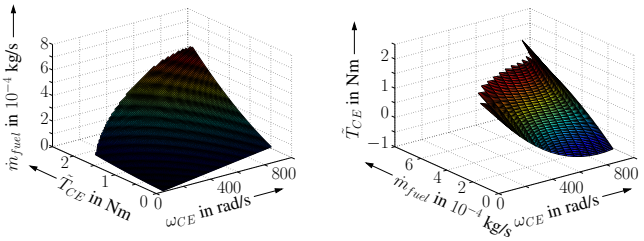

(a) Fuel consumption map. (b) Torque characteristic.

Fig. 4. Quasi-static characteristics of the internal combustion engine.

C. Conceptional Test Rig Design

To validate the numerical results that are summarized in the following sections by suitable experiments, a test rig for a small-scale combustion engine is currently being built up at the Chair of Mechatronics at the University of Rostock. In this test rig, a combustion engine (Fig. 5, left) is directly connected to an asynchronous motor (Fig. 5, right) which is operated in a torque-controlled mode. In such a way, the resulting torque T_{CE} at the combustion engine side of the gear box, see also Fig. 1, is specified as the counter torque provided by the asynchronous motor. The dynamic models for the vehicle and the gear box (including the gear shifting strategies) then have to be evaluated in real time according to the system representation described above. In such a way, it is possible to experimentally compare the influence of different gear box operating strategies and drive cycles on the fuel consumption of the internal combustion engine. Furthermore, a virtual parallel hybrid vehicle can be implemented easily on this test rig. For this purpose, the resulting torque at the gear box has to be computed online after including further real-time applicable simulation models for an electric motor-generator unit as well as for energy storage devices such as batteries. A suitable control-oriented battery model can be found in [10].

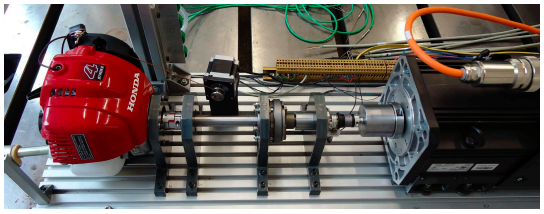

Fig. 5. Small-scale combustion engine test rig.

III. Optimization of Drive Cycles and Operating Strategies

In this section, two different optimization scenarios are taken into account. Firstly, the parameters α_{ij}, t_1, and t_2 of the drive cycle defined in (3) are optimized by a Nelder-Mead simplex method (FMINSEARCH in MATLAB) such that the overall fuel consumption is minimized with fixed gear shifting points $\underline{\omega}_{CE}$ and $\overline{\omega}_{CE}$. Secondly, the values $\underline{\omega}_{CE}$ and $\overline{\omega}_{CE}$ are optimized simultaneously with the drive cycle parameters. In both cases, the equality constraints (4)–(6) are considered exactly. Bounds on the admissible maximum values of the acceleration and velocity (cf. Subsection II-A), the path length $s\,(t_f)$, a minimum safety margin to the upper bound $\overline{T}_{CE}$ for the engine torque, a minimum distance of $\underline{\omega}_{CE}$ and $\overline{\omega}_{CE}$ as well as the prevention of positive accelerations during phase C are accounted for by additive penalty terms in the cost function corresponding to a virtual enlargement of the fuel consumption. The optimization results are summarized in Figs. 6 and 7 for both scenarios, where the fuel consumption for scenario 1 is 2.653 $\frac{\text{l}}{100\text{km}}$ and 2.407 $\frac{\text{l}}{100\text{km}}$ for scenario 2.

IV. Design of Velocity Control Procedures

A. Design of Observer-Based Cruise Control Strategies

In this section, a basic procedure is presented for tracking of desired velocity profiles in cruise control applications. Here, it is necessary to adjust the fuel mass flow provided to a combustion engine in such a way that a-priori unknown disturbances are compensated. These disturbances mainly result from the forces summarized in (7)–(9), where in practical applications neither the vehicle mass m_{veh}, the inclination angle γ of the road, the coefficients c_w for the drag resistance nor the coefficient μ for the rolling resistance are known exactly.

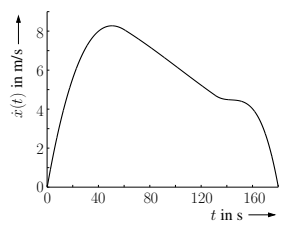

(a) Optimized velocity profile.

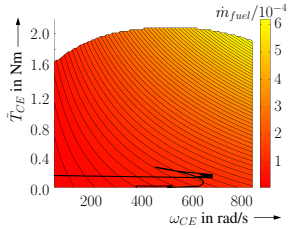

(b) Optimized operating points.

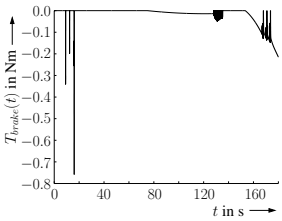

(c) Optimized velocity profile.

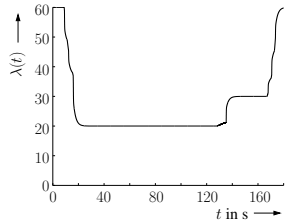

(d) Gear box transmission ratio.

Fig. 6. Optimization scenario 1.

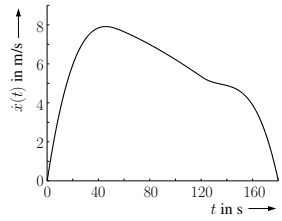

(a) Optimized velocity profile.

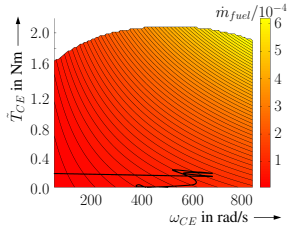

(b) Optimized operating points.

Fig. 7. Optimization scenario 2.

For these reasons, the disturbance torque acting onto the combustion engine is estimated by a suitable observer. This estimate, moreover, takes into account imprecise knowledge concerning the torque and speed dependencies of the fuel consumption map. This fuel consumption map is typically given for quasi-static operating conditions. Deviations between the quasi-static fuel consumption of the combustion engine and its dynamic operating regime are typically neglected during control design and are finally estimated together with the dynamics of the gear shift procedure to enhance the robustness.

Under these assumptions, the simplified system model that is the basis for the design of the automatic cruise control procedure is given by

$$\begin{aligned} m_{veh} \cdot r_{wheel} \cdot \ddot{x}(t) &= m_{veh} \cdot r_{wheel}^2 \cdot \dot{\omega}_{wheel}(t) \\ &= T_{GB}(t) - T_{d,veh}(t) \quad . \end{aligned} \tag{22}$$

In (22), $T_{d,veh}(t)$ represents all disturbances acting directly on the vehicle (such as air resistances or downhill-slope forces) as well as model simplifications in terms of a lumped variable.

The expression (22) is equivalent to the relation

$$\frac{m_{veh} \cdot r_{wheel}^2}{\lambda} \cdot \dot{\omega}_{wheel}(t) = T_{CE}(t) - T_{d,CE}(t) \tag{23}$$

if the gear box ratio $\lambda > 0$ is assumed to be a fixed system parameter. The corresponding disturbance torque — represented by the torque $T_{d,CE}(t)$ at the combustion engine's shaft — is estimated in the following by means of an observer (value $\hat{T}_{d,CE}(t)$). Moreover, the torque $T_{CE}(t)$ that is provided by the combustion engine serves as the system input.

It can be calculated by a linear feedback control law

$$\begin{aligned} T_{CE}(t) = \hat{T}_{d,CE}(t) &+ \frac{m_{veh} \cdot r_{wheel}^2}{\lambda} \cdot \dot{\omega}_{wheel,d}(t) \\ &+ k_p \cdot (\omega_{wheel,d}(t) - \omega_{wheel}(t)) \\ &+ k_i \cdot \int_0^t (\omega_{wheel,d}(\tau) - \omega_{wheel}(\tau))\, d\tau \quad , \end{aligned} \tag{24}$$

where $\omega_{wheel,d}(t)$ and $\omega_{wheel}(t)$ represent the desired and actual angular velocities of the wheels, respectively.

This control input is transferred to the commanded signal for the fuel mass flow according to Subsection II-A. Firstly, the quasi-static motor torque $\tilde{T}_{CE}(t)$ is determined by evaluating the transfer function given in (21). Secondly, the fuel consumption map shown in Fig. 4(a) is evaluated for the torque $\tilde{T}_{CE}(t)$ and the combustion engine's rotary speed for the steady-state gear ratio λ, that is, for

$$\omega_{CE}(t) \approx \lambda \cdot \omega_{wheel}(t) = \frac{\lambda}{r_{wheel}} \cdot \dot{x}(t) \quad . \tag{25}$$

The corresponding fuel mass flow $\dot{m}(t)$, or correspondingly its power equivalent P_{fuel}, is used as the input of the direct system model in Fig. 1.

In (24), the gain $k_p(\lambda)$ of the proportional feedback as well as the gain $k_i(\lambda)$ of the integrating feedback are determined by a gain-scheduled pole assignment with the eigenvalues $\lambda_{c,i}$, $i = 1, 2$, which are chosen to be independent of the gear box ratio λ. With this choice, the controller gains are given by

$$\begin{aligned} k_p(\lambda) &= -\frac{(\lambda_{c,1} + \lambda_{c,2}) \cdot m_{veh} \cdot r_{wheel}^2}{\lambda} \quad \text{and} \\ k_i(\lambda) &= \frac{\lambda_{c,1} \cdot \lambda_{c,2} \cdot m_{veh} \cdot r_{wheel}^2}{\lambda} \quad . \end{aligned} \tag{26}$$

The purpose of using the integrating velocity feedback is to compensate steady-state model errors which are not estimated exactly by the following disturbance observer.

The disturbance observer for the torque $\hat{T}_{d,CE}(t)$ is based on the state equations

$$\begin{aligned} \begin{bmatrix} \dot{\hat{\omega}}_{wheel}(t) \\ \dot{\hat{T}}_{d,CE}(t) \end{bmatrix} &= \begin{bmatrix} \frac{\lambda}{m_{veh} \cdot r_{wheel}^2} \cdot \left(T_{CE}(t) - \hat{T}_{d,CE}(t) \right) \\ 0 \end{bmatrix} \\ &+ \begin{bmatrix} l_{b,1} & l_{b,2} \end{bmatrix} \cdot (y_m(t) - \hat{y}_m(t)) \quad , \end{aligned} \tag{27}$$

where the second differential equation is an integrator disturbance model for the torque. This torque as well as the estimate $\hat{\omega}_{wheel}$ (which replaces the velocity $\omega_{wheel}(t)$ in (24),(25)) are determined for the vehicle velocity $y_m(t) = \dot{x}(t) = r_{wheel} \cdot \omega_{wheel}(t)$ as the measured system output with the corresponding output estimate $\hat{y}_m$. Here, again a gain-scheduled pole assignment is performed with the eigenvalues $\lambda_{o,i}$, $i = 1, 2$,

according to

$$l_b = \begin{bmatrix} l_{b,1} \\ l_{b,2} \end{bmatrix} = \begin{bmatrix} -\frac{(\lambda_{o,1}+\lambda_{o,2})}{r_{wheel}} \\ -\frac{\lambda_{o,1}\cdot\lambda_{o,2}\cdot m_{veh}\cdot r_{wheel}}{\lambda} \end{bmatrix} . \quad (28)$$

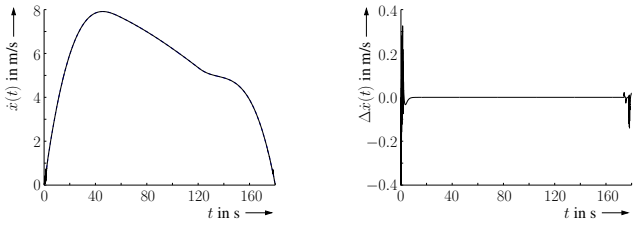

(a) Velocity profile. (b) Control error.

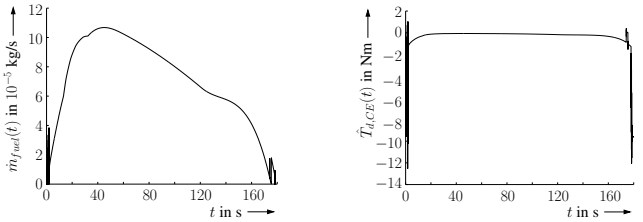

(c) Fuel mass flow. (d) Disturbance estimate $\hat{T}_{d,CE}$.

Fig. 8. Results of observer-based velocity control.

B. Nonlinear Internal Model Control (IMC)

As an alternative to the observer-based velocity control presented in Subsection IV-A, an IMC structure can be employed. In an underlying control loop, the vehicle's speed is asymptotically stabilized by the proportional control law

$$\tilde{T}_{CE}(t) = \tilde{T}_{CE,IMC}(t) - k_p \cdot \omega_{wheel}(t) \quad , \quad (29)$$

which, however, does not guarantee tracking of desired velocity profiles and compensation of unknown disturbances. Here, the controller gain k_p is chosen according to

$$k_p(\lambda) = -\frac{\lambda_c \cdot m_{veh} \cdot r_{wheel}^2}{\lambda} \quad (30)$$

with a fixed desired eigenvalue λ_c of the closed control loop.

The IMC control part of the torque $\tilde{T}_{CE}(t)$ is given by

$$\tilde{T}_{CE,IMC}(s) = \frac{\frac{m_{veh}\cdot r_{wheel}^2}{\lambda}\cdot s + k_p(\lambda)}{T_{IMC}\cdot s + 1} \cdot \Delta\Omega(s) \quad , \quad (31)$$

where $\Delta\Omega(s)$ corresponds to the Laplace transform of the control error $\Delta\omega = \omega_{wheel,d}(t) - \omega_{wheel}(t) + \hat{\omega}_{wheel}(t)$ with the sufficiently small time constant T_{IMC} guaranteeing causality of the transfer function in (31). The term $\hat{\omega}_{wheel}(t)$ results from evaluating the simplified parallel model of the plant (23) for the input torque $\tilde{T}_{CE}(t)$, where the disturbance torque is set to zero.

The excellent tracking performance of both controllers can be seen in Figs. 8 and 9, where $\gamma(x) = 0.1 \cdot \sin(0.01 \cdot x)$ is used to simulate disturbances. In both cases, the fuel mass flow is adjusted by an additive term $K_f \cdot \int_0^t T_{brake}(\tau)d\tau$ (s.t. $\dot{m}_{fuel} \geq 0$) to minimize the braking effort if a fuel mass flow is computed which is unnecessarily large.

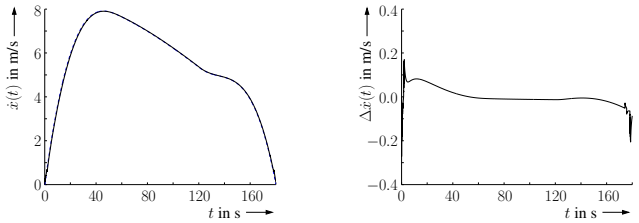

(a) Desired velocity (dashed); actual velocity (solid). (b) Control error.

Fig. 9. Results of nonlinear internal model control.

V. Conclusions and Outlook on Future Work

In this paper, different optimization approaches have been presented for the minimization of the fuel consumption of combustion engine-based power trains. Especially, the offline planning of optimal velocity profiles for vehicles which are operated according to a fixed timetable leads to a significant reduction of the fuel consumption if the switching points for gear shifting are adapted accordingly. In such a way, it is possible to operate the combustion engine in the point of its minimal fuel consumption. Additionally, the corresponding system models have been used to design cruise control procedures which can be employed to follow predefined velocity profiles in spite of disturbances such as a-priori unknown downhill-slope forces.

To exploit the advantages of optimal control also in this case, future work will deal with an online adaptation of the vehicle's operating strategy according to a real-time model predictive control procedure. Moreover, future work aims at the implementation of all control and observer procedures on a corresponding test rig at the Chair of Mechatronics at the University of Rostock according to Subsection II-C.

References

[1] L. Guzzella and C. Onder, *Introduction to Modeling and Control Combustion Engine Systems*. Springer-Verlag, 2010.

[2] L. Guzzella, *The QSS Toolbox Manual*. ETH Zürich, Institute for Dynamic Systems and Control, 2010.

[3] L. Guzzella and A. Sciarretta, *Vehicle Propulsion Systems. Introduction to Modeling and Optimization*. Springer-Verlag, 2005.

[4] M. Fliess, J. Lévine, P. Martin, and P. Rouchon, "Flatness and Defect of Nonlinear Systems: Introductory Theory and Examples," *Int. J. Control*, vol. 61, pp. 1327–1361, 1995.

[5] M. Leska, R. Prabel, A. Rauh, and H. Aschemann, "Simulation and Optimization of the Longitudinal Dynamics of Parallel Hybrid Railway Vehicles," in *Proc. of FORMS/FORMAT-2010, Part 2*, E. Schnieder and G. Tarnai, Eds. Springer, 2011, vol. 281, pp. 155–164.

[6] M. Leska, T. Grüning, H. Aschemann, and A. Rauh, "Optimization of the Longitudinal Dynamics of Parallel Hybrid Railway Vehicles," in *IEEE Multi-Conference on Systems and Control*, Dubrovnik, Croatia, 2012.

[7] B. Saerens, M. Diehl, J. Swevers, and E. Van den Bulck, "Model Predictive Control of Automotive Powertrains — First Experimental Results," in *IEEE Conference on Decision and Control*, Cancun, Mexico, 2008, pp. 5692–5697.

[8] J. Löffler, "Optimierungsverfahren zur adaptiven Steuerung von Fahrzeugantrieben," Ph.D. dissertation, University of Stuttgart, Germany, 2000, in German.

[9] S. Terwen, "Vorausschauende Längsregelung schwerer Lastkraftwagen," Ph.D. dissertation, KIT Karlsruhe, Germany, 2009, in German.

[10] A. Rauh and H. Aschemann, "Sensitivity-Based State and Parameter Estimation for Lithium-Ion Battery Systems," in *Proc. of Intl. Conference System Identification and Control Problems SICPRO'12*, Moscow, Russia, 2012, ISBN 978-5-91450-098-3.